Atmospheric Turbidity Measurements at Broome
in
Western Australia 1979-1984

W D Scott[1], B W Forgan[2], & J M Prospero[3]

[1]School of Biological and Environmental Sciences, Murdoch University, Murdoch WA 6150.
[2]Bureau of Meteorology Research Centre, Melbourne, VIC 3000.
[3]Cooperative Institute for Marine and Atmospheric Studies, Miami, Florida, 33149 USA.

Abstract

A special version of a Voltz, hand-held sun photometer was used to measure direct solar radiation several times each day at the meteorological station at Broome aerodrome from 1979 to 1984. These data were fully compensated and corrected and interpreted in terms of atmospheric turbidity using precise solar calculations. Calibration included extrapolation to zero air mass (Langley plots) and cross-comparisons. The data show no synoptic or mesoscale variation but a seasonal variation with higher values near the end of the dry periods. Calculated wavelengths exponents show smaller particles are present in these dry periods. A harmonic analysis shows that 20-25% of the variance is explained by an annual cycle, 10-15% by a cycle of 3 years, and that turbidity increases 7-11% per year. Bushfires and marine aerosols are likely to be important contributions to the trends though effects of the volcanic eruption of Galunggung are apparent in 1982-1983.

Introduction

The occurrence of dust storms from the Australian continent and the movement of volcanic dust clouds through the area is important on a global scale. It is known that dust storms over Australia inject large quantities of mineral aerosols into the atmosphere during the September-October and February-March periods (Middleton 1984). Dust clouds have been known to spread out in a plume that covers a large portion of the Indian Ocean (Bell 1991, McTainsh *et al*. 1989). The importance of this quantity of aerosol to the radiation budget of the area and the global energy budget should not be underestimated (Kondratyev 1972).

Burning is another concern; it raises elemental carbon and, through subsequent photochemistry, ozone levels. A spring maximum from biomass burning may be propagated throughout the southern hemisphere (Heintzenberg & Bigg 1990). A seasonal cycle in ozone is observed over Indonesia with a maximum in the March-April period when biomass burning is most common (Fishman *et al*. 1990). The Kimberley area of Western Australia is frequently heavily burnt; the area burnt by each individual fire increases with time after cessation of the rainy season (Bell 1981, Haynes 1985). In late 1984 a bushfire plume was evident over Broome (J L Gras personal communication).

In addition, during the period 1979-1984 a number of eruptions of volcanos affected the turbidity (τ) or Aerosol Optical Depth (AOD; considered identical to turbidity in this paper) in the southern hemisphere. The major eruption of El Chichon in Central America in April 1982 has been shown to have affected stations in the Antarctic (Etheridge 1984). Several Indonesian volcanos were also active in 1982 (Scientific Event Alert Network 1981, 1982). The stratospheric aerosol level increased from late 1982 through to 1984 from these volcanic eruptions (Gras *et al*. 1986). In particular, eruptions of the volcano Galunggung in Indonesia produced ash clouds that were shown to have passed

directly over Broome in July 1982. A study of the passage of the Galunggung and El Chichon plumes over Broome and the relative values of τ during their passage should help quantify the way volcanic aerosols move and disperse. Such aerosols not only decrease the intensity of solar radiation but also damage high flying aircraft (Creagh 1992).

With the conception of the Global Weather Experiment a number of aerosol monitoring stations were established around the globe. Along with other instruments these stations contained sun photometers modelled after the design of Voltz (1959). One such station at Broome in the northwest of Western Australia measured the intensity of direct solar radiation from May 1979 to November 1984. This data set is one of the longest consistent measures of turbidity in the southern hemisphere. This paper describes the calibration procedures used on the instruments and reports the calculated values of τ (AOD) and the wavelength exponents. The results are interpreted in terms of known volcanic activity and cyclic trends in the troposphere and stratosphere.

Materials and Methods

Location and Meteorology

Broome is located at 17° 57′ S latitude and 122° 15′ E longitude and generally experiences the wet and dry periods of the tropics in southern latitudes. During the wet half of the year (December to April) the surface low pressure area over the inland tropics produces low level west to southwest winds over the Broome area. The surface wind flow is characterised by a generally light to moderate flow that is strengthened near the coast by a sea breeze. At atmospheric pressure levels between 850 to 500 mb winds are predominantly easterly. Tropical depressions and cyclones occasionally affect the area in this period and often result in strong easterly winds at all levels below 500 mb. In the dry half of the year the middle latitude ridge moves northwards and consequently easterly winds prevail below 850 mb while westerlies dominate above this level.

The Sun Photometer

The instruments used in the study are improved versions of the instrument of Voltz (1959). Instrument specifications are listed in Table 1. Note that the photometers are hand-held and a scanning procedure is used to detect the direct radiation coming from the sun. A peak sample-and-hold circuit is used to store the maximum measured signal from the silicon photosensor. The sensors are affected by temperature with approximately 0.1% change in response per degree Celsius. The temperature drift of each sensor is given by the manufacturer and was remeasured at the University of Miami (by Tom Snowdon) and a linear regression line fitted to data. In-field compensation was achieved by a thermistor thermometer built into the units. A FORTRAN program interpreted the maximum voltage measurement after compensating for temperature, and calculated the precise solar position and the final value of τ. Various versions of this program were generated by David Pascoe, William Scott and Bruce Forgan (see Acknowledgements and Herman *et al.* 1981).

Table 1

Specifications of the University of Miami
Series 300 Sun Photometer

Interference Filters:
  (Located in filter wheel)
  Red*—875 nm with 16 nm half width
  Green—500 nm with 10 nm half width
  Blue—380 nm with 11 nm half width.
  manufactured by Microcoatings, Inc.
  * bonded to a disk of UG1 Schott glass 1 mm thick for Infrared
    cut-off.

Detector:
  (Located 8 cm behind the filter wheel)
  Bell & Howell type 529-2-5
  Silicon Photodiode of 5 mm area.

Optics:
  Approximately a 2° viewing angle in UM 321. Photometer UM 318 has a viewing angle of 1°, achieved by adding a 271 mm tube with a front aperture 7.14 mm in diameter.

Two different instruments were used in the study: UM321 from May 1979 to July 1981, and UM318 from July 1981 to November 1984. Photometer 318 was identical to 321 except that it was fitted with an additional optical tube to provide a viewing angle of 1 degree. This tube improved the sensitivity and stability of the optical depth measurements. Both instruments measured the intensity of direct solar radiation at four wavelengths: Blue (380 nm), Green (500 nm), Red (880 nm), and Water (945 nm); the near infrared Water (945 nm) measurements are not reported here. Filter characteristics are listed in Table 1.

Measurements were taken when possible in the early morning, midday and late afternoon. This allows for partial *in situ* calibration should there be a temporal change in the instrument electronics or optics (J M Prospero, 1978: Manual for Series 300 RSAMS Sun Photometers, unpublished).

Calibration

The two instruments were calibrated in 3 ways:

1. Langley plots before and after the experiments and during comparison experiments

2. Daily *in situ* calibration

3. Cross-calibration with one another and standards.

The Langley analysis assumes a constant optical depth during the measuring period (usually one day); plotting the output voltage as a function of known air mass allows the values of the voltage that would be measured at zero air mass (J_0) to be obtained by extrapolation. At the chosen wavelength this voltage corresponds to the sun's intensity outside the atmosphere at a mean sun-earth distance (Kondratyev 1972).

Langley plots of the instruments' response were completed on several occasions including pre-use and post-use. Fig 1 shows the extrapolation for 11 February 1981, 13 February 1981 and 13 April 1983 for photometer UM321. Note that data from 14 February 1981 overlayed the data of 11 February 1981 and are not shown. The resulting calibration J_0 constants are listed in Table 2. These measurements are made at different wavelengths; they must be made on relatively clear days with a consistent τ. In addition, especially at low sun elevation, the time between measurements should be less than 1 minute. The statistics of the calibration should follow Herman *et al.* (1981). Practically it is found that refractions and local effects become important above air mass 2.5; it is preferable to have at least 5 measurements at equally spaced intervals between air mass 1 and 2.5.
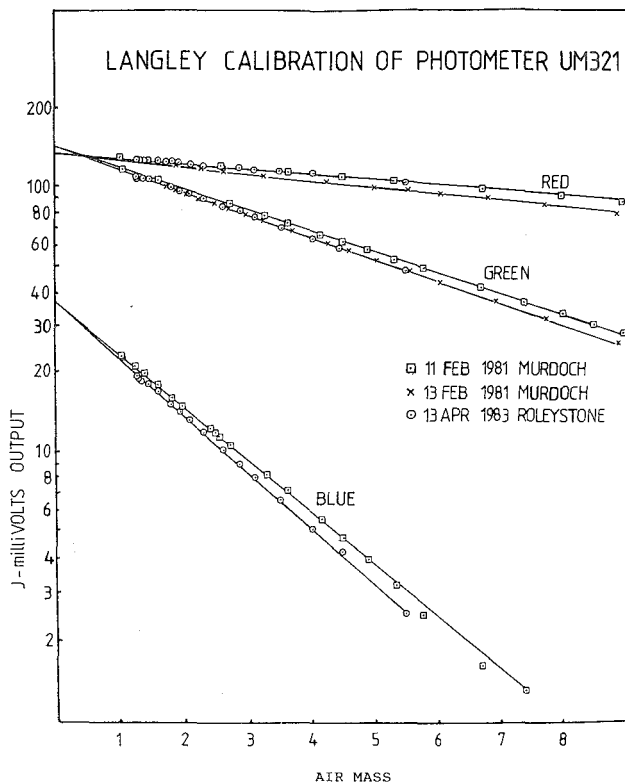

Figure 1 Extrapolation of the measured output of photometer UM321 to zero air mass. This Langley analysis produces the calibration J_0 values (see Voltz 1978).

Calibration data were also obtained by using daily *in situ* data collected at Broome. With typically six data cycles per day, the Langley method was used on the limited morning and afternoon data cycles, hereafter called the short Langley technique. Data were edited to remove those days in which the morning and afternoon total optical depths, derived from the short Langley analysis, were markedly different, or less than the assumed molecular optical depth (see end of section for an explanation). *In situ* calibrations

Table 2

Results of Langley Calibrations for J_o

Instrument	Filter				Form used for data— Based on *in situ* calibration
		Original Calibration[1]	February 1981	13 April 1983	
	Blue (380 nm)	41.2 mv	38	37	38.2
UM321	Green (500 nm)	159.5 mv	143	140	151.1 – 4 (T-1979)
	Red (880 nm)	135.3 mv	134	134	133.2
			11 May 1981	22 December 1984	
	Blue (380 nm)		58.4	42	55.13 – 1.866 (T-1981)
UM318	Green (500 nm)		201.6	199	202.4 + 1.484 (T-1981)
	Red (880 nm)		174.6	165	169.4 – 0.6 (T-1981)

[1] University of Miami (1978).

were then performed on all data for the remaining days (air masses below 6.0). The resulting extrapolations were then averaged for the month. These produced consistent trends in the calibrations at several wavelengths. These trends were statistically significant and were used in the processing of the data.
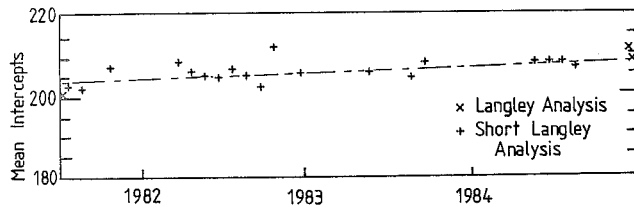

Figure 2 Comparison of the *in situ* values for J_o from the short Langley analyses with the values for pre- and post-Langley analysis.

The *in situ* results compared well with the Langley analyses prior to and after collection of the data set. A plot of the results of the short Langley analysis for UM#318 at 500 nm is shown in Fig 2, together with the values derived from special Langley calibration analyses mentioned above. The upward trend evident in the figure proved to be a function of the gradual rotation of the sensor by mechanical vibration over an extended period. When returned to its original position, the 500 nm calibration returned to within 1 per cent of the original 1981 Langley calibration.

Cross calibrations were completed when the instruments were traded and at the end of the sampling period. These amounted to making nearly simultaneous measurements. As expected, the correlations between like wavelengths were high in each series and confirmed the drift shown by the other calibration methods. The correlation coefficients between photometers UM318 and UM321 on 10 June 1981 ranged between 0.95 and 0.98; on 22 December 1984 between 0.93 and 0.97.

Additional comparisons with state-of-the-art World Meteorological Organisation (WMO) design sun photometers, at the Cape Grim Baseline Air Pollution Station in Tasmania, also confirmed the end calibration values, after small corrections were made for the difference in central wavelengths.

Processing the Data

A precise algorithm (developed by B Forgan and D Pascoe), was used to obtain the zenith angle of the sun θ and the mean earth-sun distance. Then the air mass, m = secant θ, was used to obtain the optical depth at the mean earth-sun distance at m = 1.0:

$$\tau = \frac{\ln J/J_o}{m} \tag{1}$$

where J is the measured signal and J_o the calibration constant related to the true earth-sun distance. Corrections were made for ozone absorption and molecular scattering affects by subtraction.

The molecular optical depth was determined from the functional form given by Frohlich and Shaw (1980) but with corrections determined by Young (1981). Ozone coefficients were those recommended by the World Meteorological Organisation (1982).

During the period of very low τ, a small number of the derived values were either zero or negative. These data were ignored in the analysis presented below. Quality control analyses suggest that the negative values occurred through unaccountable instrument drift or transcription error (see Discussion). For a single observation at unit airmass, error analysis suggests a precision of 0.010 in the results for τ_{500}, 0.020 for τ_{380} and 0.006 for τ_{875}.

The data were later interpreted using a harmonic analysis and a separate frequency analysis. Bloomfield (1976) presents the procedures for both techniques. The analyses were completed using a Vax 780 computer at the University of Miami using library routines for the required FFT (Fast Fourier Transform) analysis and matrix inversions. The harmonic analysis fits the data to a set of frequencies that are multiples of the lowest frequency (about 5.5 year) using as many harmonics as are required to sensibly fit the data. It is a standard technique but suffers from the compounding of errors when solving for a large number of harmonics and doesn't allow for frequencies other than multiples. The frequency analysis is a trial and error method that picks the most significant frequencies independent of whether they are multiples or not. In both types of analysis, the fit gives a minimum of the sum of the squares of the deviations, a 'maximum likelihood' estimation. The frequency analysis is tedious but minimises the calculation error and can easily allow for non-cyclic trends in the data (linear and exponential).

Results

All the data are plotted in Fig 3 as single points relative to the time of day. Note that there is little, if any, preference for higher τ in any part of the day although most measurements were made slightly after solar noon. Several averages were calculated to separate the trends in these data. Fig 4 shows average daily values for the whole measurement period. Other average values are presented in Figs 5, 6, 7 and 8. The lines in Figs 6, 7 and 8 simply connect average values.
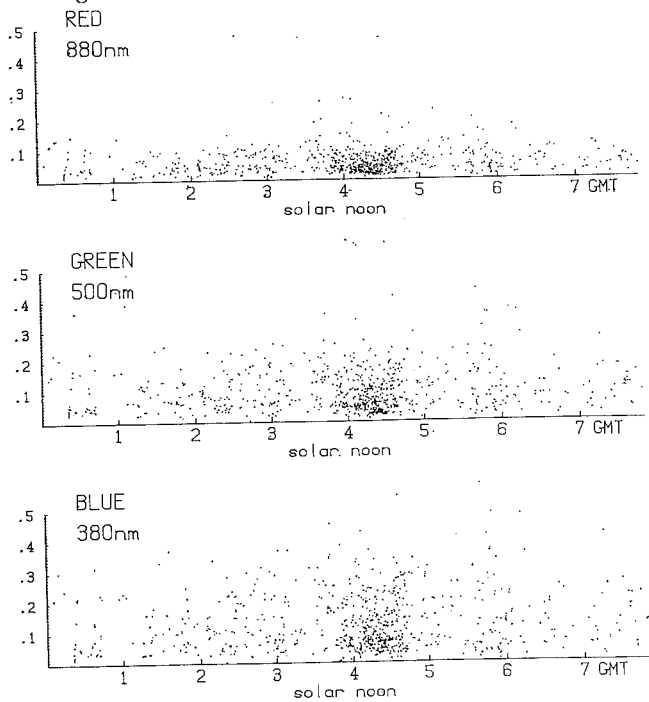

Figure 3 Atmospheric turbidity (τ) values measured at the Broome Aerodrome. All values measured between 1979 and 1984 are plotted as a function of the time of the day.

Generally, few data points were collected in the months of December, January and February because of the high cloudiness. The March and April data dominate. Lowest values occur from April through July; highest, September through November. The values for September through November are typically 2.3 times the values observed from April through July, for all wavelengths. For example, τ_{500} ranges typically from 0.05 in winter to 0.125 in spring.

The seasonal trends of Fig 4 are clear in the overlay of data in Fig 5. Note that these points are weekly averages and the same symbol, rotated, is used for all years. Little, if any of the variation is removed by this averaging; even the monthly averaged values of Fig 6 exhibit most of the variation. Only with yearly averaging (Fig 7) does the variation diminish significantly.

Wavelength exponents:

$$\alpha_{BR} = \frac{-\ln (\tau_{Blue}/\tau_{Red})}{\ln (380/880)} \qquad (2)$$

$$\alpha_{GR} = \frac{-\ln (\tau_{Green}/\tau_{Red})}{\ln (500/880)} \qquad (3)$$

give some information on the size distribution of the aerosol particles. They were calculated for each measurement and averaged over various periods. Fig 8 shows monthly averages of these quantities on the lower two
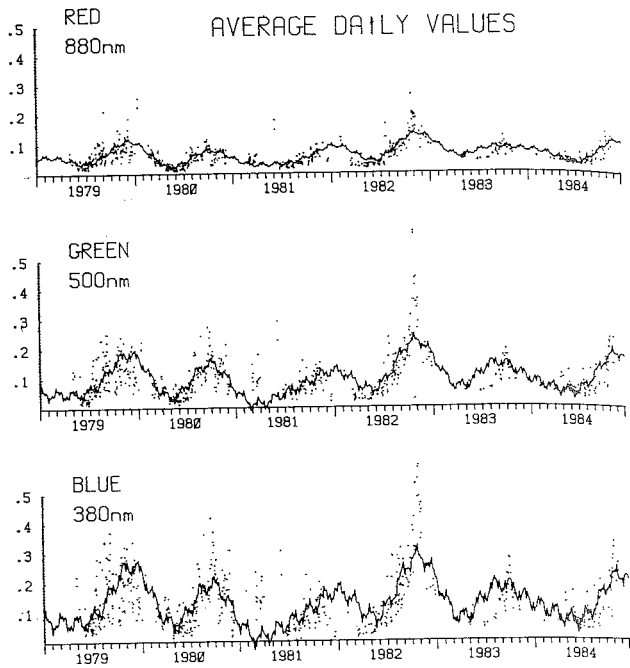

Figure 4 Average daily values of τ measured between 1979 and 1984 at Broome, Western Australia. Fitted curves from the frequency analyses are included (see Table 3).
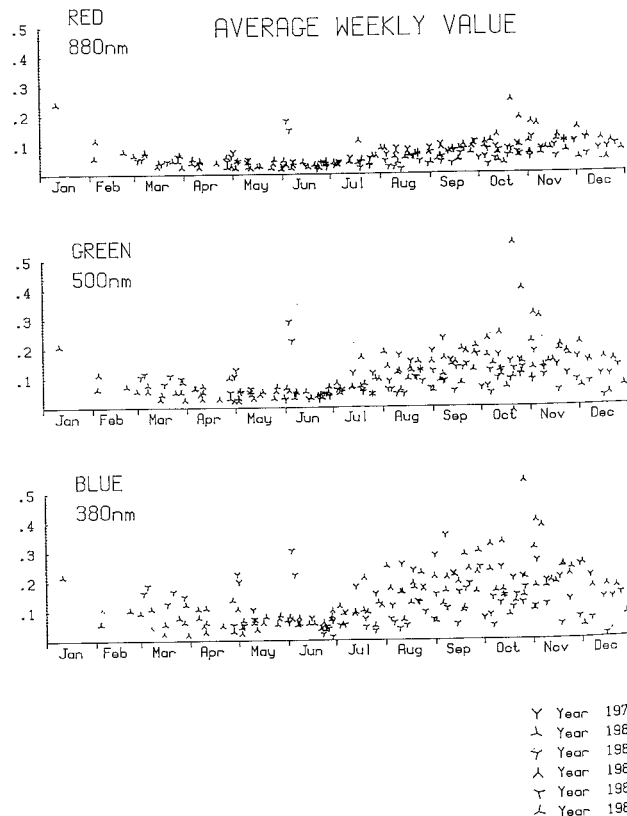

Y Year 1979
⋏ Year 1980
⋎ Year 1981
⋏ Year 1982
⋎ Year 1983
⋏ Year 1984

Figure 5 Average weekly values of τ measured between 1979 and 1984 at Broome, Western Australia.
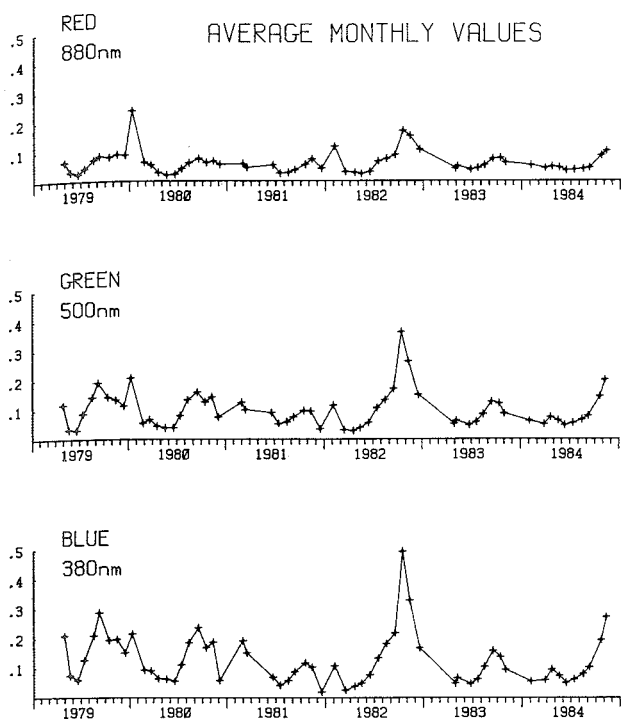
114

Figure 6 Average monthly values of τ measured between 1979 and 1984 at Broome, Western Australia. Lines join the average monthly values.
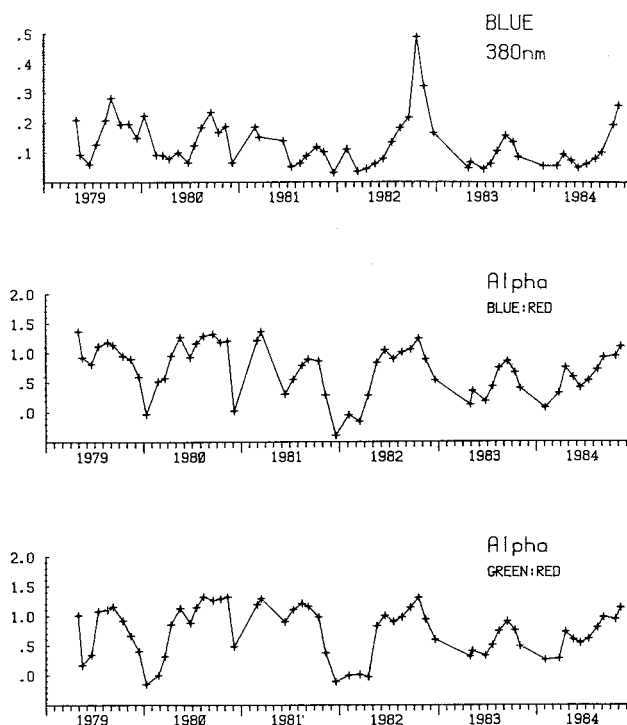

Figure 8 Monthly averaged values for wavelength exponents (α) measured between 1979 and 1984 at Broome, Western Australia are presented on the lower two curves; the τ measured with the blue filter is displayed on the upper curve for comparison.
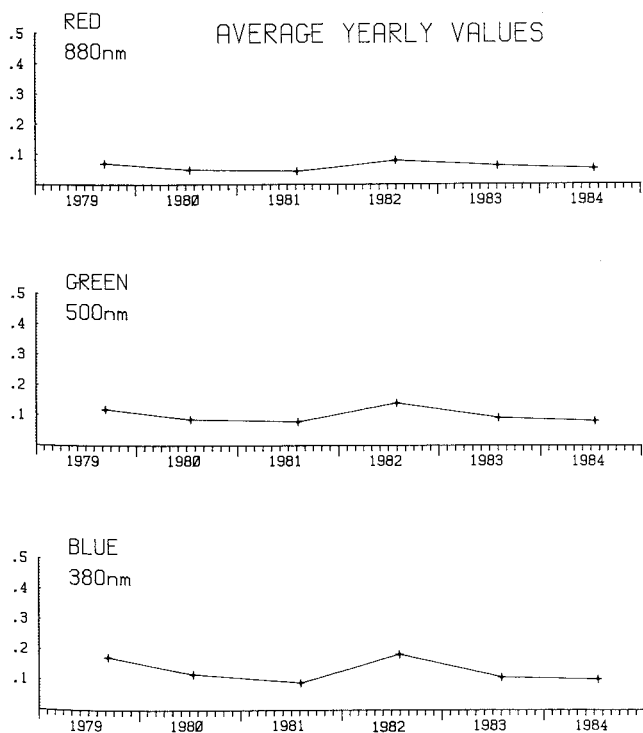

Figure 7 Average yearly values of τ measured between 1979 and 1984 at Broome, Western Australia. Lines join the average yearly values.

curves. A plot was also made of the Blue : Green wavelength exponent; the green values exhibit some anomalies and the combination Blue : Green produced some large negative values of α. Also τ values less than 0.02 were excluded because of the large influence of small (nearly zero) values on the ratios.

The derived α means were lower during April through June for all wavelength pairs. Larger values (greater than unity) occur during September through November. The uncertainties of the α values depend on the season and wavelength pair. A value of 0.25 is a conservative estimate of the error in monthly mean α for all wavelength pairs. The differences between monthly mean α from March-June and August-November periods are 0.3 for α_{BR} and 0.4 for α_{GR}.

The cyclic or nearly cyclic variations in the τ data suggest that a harmonic analysis or a frequency analysis might be appropriate. The harmonic analysis included as many as 50 harmonics and explained as much as 70% of the variance in the data. The effectiveness of the analysis for the Blue optical depth data is represented in Fig 9. Here the number of harmonics is plotted on the abscissa; these are harmonics relative to the entire data set with a period of 5.5549 years or 0.18 cycles/year. The entire data set of approximately 2900 data points yields 643 separate daily average values. The Coefficient of Determination (COD; r^2) is plotted on the ordinate. Note that, in fact, substantial improvements in COD only occur when frequencies of periods 2-3 years, $\cong 1$ year, and $\cong 0.5$ years are fitted to the data; most of the variance in the data is explained by these harmonics. Hence a further frequency analysis was completed following the

115

method of Bloomfield (1976). This considers selected frequencies that affect the standard deviation and includes a constant and a linear trend. Table 3 is a summary of the results when seven frequencies are allowed;

$$X(t) = \mu + nt + \sum_{j=1}^{7} (A_j \cos \omega_j t + B_j \sin \omega_j t) \qquad (4)$$

The analysis uses a trial-an-error fitting procedure to minimise the sum of the differences (maximum likelihood). here, μ is the mean and n is the linear trend. Seven frequencies were sufficient to fit the data. An annual cycle explains 20-25% of the variance (Table 3).

Table 3

Results of the frequency analysis for atmospheric turbidity in Broome, 1979-1984

	Period	Coefficient	Phase[1]	% Variance explained
Blue (380 nm) (average = 0.1370, sd = 0.1088)				
Mean (μ)[2]		0.1036		
Linear Trend/yr (n/μ)[2]		+0.0075		
		(+7.2%/yr)		
1st frequency	1 year	0.06551	-152°	20%
2nd frequency	2.91 years	0.05124	-61°	11%
3rd frequency	0.716 yrs	0.03471	68°	5%
4th frequency	1.89 mo	0.02303	2°	2%
5th frequency	4.3 days	0.01314	-10°	0.7%
6th frequency	7.5 days	0.01221	89°	0.6%
7th frequency	5.8 days	0.01144	-45°	0.6%
COD = 0.45				
Green (500 nm) (average = 0.1028, sd = 0.07605)				
Mean (μ)[2]		0.0732		
Linear Trend/yr (n/μ)[2]		+0.0080		
		(+11%/yr)		
1st frequency	1 year	0.05112	-155°	25%
2nd frequency	2.91 yrs	0.03483	-62°	11%
3rd frequency	0.714 yrs	0.02516	57°	5%
4th frequency	1.89 mo.	0.01341	7°	2%
5th frequency	5.8 days	0.00784	-43°	0.5%
6th frequency	7.5 days	0.00737	86°	0.5%
7th frequency	4.4 days	0.00724	16°	0.5%
COD = 0.48				
Red (880 nm) (average = 0.05933, sd = 0.03853)				
Mean (μ)[2]		0.04655		
Linear Trend/yr (n/μ)[2]		+0.0051		
		(+11%/yr)		
1st frequency	1 year	0.02677	177°	26%
2nd frequency	3.05 yrs	0.02045	-38°	15%
3rd frequency	0.715 yrs	0.01526	58°	6%
4th frequency	1.66 mo.	0.00598	-57°	1%
5th frequency	4.38 days	0.00383	103°	0.5%
6th frequency	7.52 days	0.00308	44°	0.3%
7th frequency	6.55 days	0.00303	-46°	0.3%
COD = 0.56				

[1] The phase is relative to the start of 1979. Note that the phase and significant digits are retained to calculate the cyclical waveform in Figures 4 and 10.

[2] see equation 4.

Of course, it is not possible to resolve whether the trend is part of a longer term variation. The three-year trend itself is of doubtful validity in only a five-year time series.

The higher frequencies are only included for interest; they appeared in the objective analysis but are unlikely to be significant. Several simulated data sets with known periodicities and the same temporal sequence were subjected to the same analysis; the result was an error of about 5% in the coefficient and 10% in the variance.
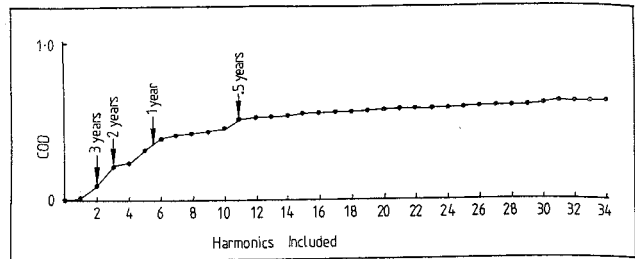

Figure 9 The Coefficient of Determination (COD; r^2) produced by the inclusion of various harmonics in the harmonic analysis of blue optical depth data.

The results of the frequency analysis were used to produce the curves shown in Fig 4 and Fig 10. These curves are produced by recombining the cyclic terms and the linear terms to produce a cyclic curve. Using the data in Table 3, the entire data set can be reproduced as the line presented in the graph. The most significant variations are shown by using the three most significant frequencies and the linear trend, as shown in Fig 10. The more oscillatory line in Fig 4 is produced by using all seven frequencies; the daily averaged data are also shown. The fit is acceptable but there is no justification for incorporating the high frequency variations.
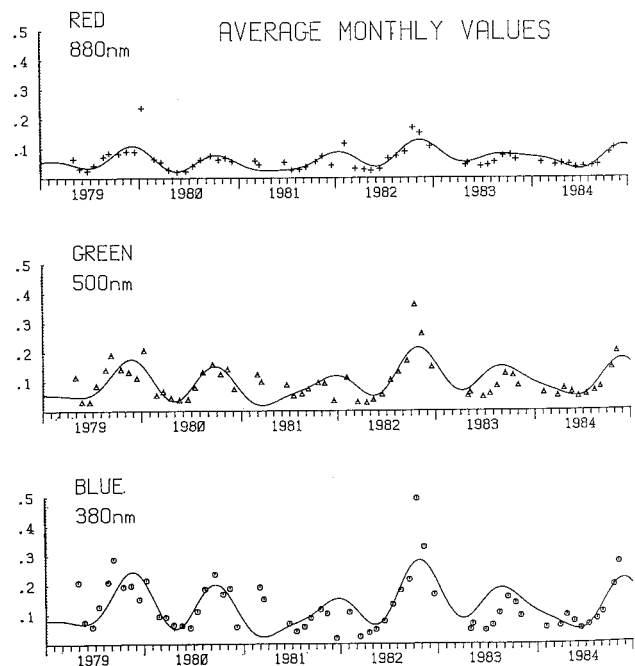

Figure 10 Fit of the data with a frequency analysis using only the three most significant frequencies (see Table 3). Data points are monthly averaged values of τ (see Fig 6).

Discussion

The seasonal nature of the atmospheric turbidity data is clear from Fig 10 where the points represent monthly averages. The variation from one year to another is marked, especially in the onset and duration of the maximum in the dry period.

The aerosol optical depths are influenced by at least two temporally dependent processes. Seasonal changes in the winds with aeolian generation of aerosol and bushfires or man's activities, and longer term trends due to stratospheric containment. The first influence is likely to be cyclic; the latter, single near random injections that gradually die through slow exchange with the troposphere. It is clear that local mesoscale trends or synoptic trends are insignificant in the data. Specifically, the objective fitting procedures (see Table 3) reveal that less than 2% of the variance can be explained by such trends. The annual cycle is easily accepted but the three year cycle is not. Though this longer cyclic effect may even be derived from some northern hemispheric influence, it is most likely a result of two or more volcanic eruptions in 1979 and 1982. Pulse injections effectively contain every possible wavelength and with time and dispersion the longer harmonics are all that remain.

The annual cycles of aerosol optical depth and wavelength exponent suggest a predominance of smaller particles in the aerosol during dry periods with a maximum in aerosol optical depths at all wavelengths. This has been observed by Angstrom (1970) in broad-band turbidity studies of northern hemisphere stations. Similar trends were also observed by Forgan (1977) in continental Australia. In the wet periods, about the end of each year, minimum values of α occur (see Fig 8). The maxima in α may result from the greater infusion of continental aerosol and the increased bio-activity and burning of the dry period. The minima in turbidity and wavelength exponent with the onset of the wet period is influence by removal or aggregation of smaller particles by moist processes.

Contributing also is the marine air mass that passes over Broome in the wet season (see Fig 4), December to April, when surface winds are from the Indian Ocean, and large salt particles predominate in the clean, maritime air. Later, in the dry season, burning-off effects are likely to contribute an ever-increasing amount of aerosol. There is an increase in turbidity and an increase in α, just before December. The dramatic pulse in turbidity observed in the September-November period of 1982 shows no apparent influence on the wavelength exponent. Though this pulse is likely stratospheric and volcanic, it is similar in overall size to the continental aerosol.

The data from 1982 and 1983 (see Fig 6) were affected by the injection of volcanic aerosol that derived from a series of eruptions from volcanos Galunggung (Indonesia) and El Chichon (Mexico). The 1983 effects are carried over from eruptions in late 1982. Satellite evidence of the influence of Galunggung volcanic plumes in the stratosphere on the radiation budget of western Australia has been reported by Bell (1983). The influence of El Chichon on global radiative transfer has been examined in numerous studies (see Bandeen and Fraser 1982). The data presented by Spinhirne (1984) for southern latitudes in October 1982, suggested that the effect of the El Chichon had reached 35°S. Evidence obtained from the Broome record suggests initial increases in τ from July to September 1982 at 20°S could be related to the large eruptions from Galunggung and that the dramatic influence of El Chichon was only evident in late October (Scientific Event Alert Network 1982). The temporal extent of the increase in aerosol optical depth can also be attributed to the simultaneous passage of the El Chichon cloud band south of 20°S. Aerosol optical depth data for 500 nm reported by Francey and Forgan (1986) for Cape Grim in Tasmania at 41°S, also shows an initial increase over the background level of between 0.05 and 0.07 to September, 1982. At Broome the major increase occurred in late October, while at Cape Grim the major increase attributed to El Chichon occurred in February 1983. The magnitude of the increase in τ at Cape Grim is of a similar magnitude to the November data at Broome.

It is important to recognize the limitations of the data set. Errors in the data are around 0.01 in τ which is small in comparison to most of the values recorded. This remains, however, a limit to the analysis and values of τ approaching 0.01 may contain gross errors.

Turbidities were not measured in cloudy conditions and would have little value. Hence, since the summer tends to have more clouds and clouds tend to occur in Broome in the mornings, there is a seasonal bias. This appears profoundly when a calibration data set of known frequency is analysed using the time sequence of the real data, giving the 10% error already mentioned. Also, a glance at the figures reveals that data are missing for nearly every year in the December-January period. This particular flaw would tend to raise the average τ since the τ values are low in this period. Some adjustment is made for this with the least squares procedure—note that the constant values in Table 3 are somewhat lower than the full averages; it is possible that the constant values from the frequency analysis are better estimates of the average τ values. The irregular nature of the data may also result in aliasing effects with anomalous harmonics appearing in the data. This should, however, be a small effect since the data were acquired at intervals of about a day and there appears to be no significant frequencies higher than one month.

It is rewarding that the sets of data at different wavelengths (Fig 6) show the same trends and that the frequency analysis produces nearly the same primary frequencies in all the data. Frequency analysis only account for about 50% of the variance observed and it appears that any reasonable harmonic analysis cannot improve on this. The remaining variance is physically acyclic, a result of instrument drift or abrupt changes, or simply random operator error. Still, the three companion measurements should, together, produce relatively valid trends and the shear number of measurements should have minimized random effects.

References

Angstrom A K 1970 On determination of the atmospheric turbidity and their relation to pyrheliometric measurements. Advances in Geophysics 14: 269-283.

Bandeen W R & Fraser R S 1982 Radiation effects of the El Chichon volcanic eruption: preliminary results concerning remote sensing. National Aeronautics and Space Administration Technical Memo 84959, Goddard Space Flight Center, Maryland.

Bell A 1981 Fire damages top-end forests. ECOS 30:18-20.

Bell A 1983 Satellite images of the volcanic ash clouds. ECOS 35:32.

Bell A 1991 Wind erosion: the winnowing of our soils. ECOS 66:4-9.

Bloomfield P 1976 Fourier Analysis of Time Series, The Search for Periodicity. Wiley, New York.

Creagh C 1992 Avoiding volcanic clouds ECOS 70: 36.

Etheridge D M 1984 Volcanic dust detection from aerosol optical depths over Dome, Antarctica. In: Australian National Antarctic Research Expedition (ANARE) Research Notes 28, Australian Glaciological Research 1982-1983 (ed T H Jacka). Symposium on Satellite Remote Sensing, Melbourne.

Fishman J, Watson C E, Larsen J C & Logan J A 1990 Distribution of tropospheric ozone determined from satellite data. Journal Geophysical Research 95:3599-3617.

Forgan B W 1977 The measurement of solar irradiance. Research Report 27, Flinders University Institute for Atmospheric and Marine Science, Bedford Park.

Francey R J & Forgan B W 1986 Baseline 1983-1984. Bureau of Meteorology, Melbourne.

Frohlich C & Shaw G 1980 New determination of Rayleigh Scattering in the terrestrial atmosphere. Applied Optics 19:1773-1775.

Gras J L, Bigg E K, Michael C G, Adriaansen A & Swinton R 1986 Stratospheric aerosol at 34°S following the 1982 El Chichon and Galunggung eruptions. Tellus 38B:67-73.

Haynes C D 1985 The pattern and ecology of munwagi traditional Aboriginal fire regimes in north central Arnhemland, In: Ecology of the Wet-Dry Tropics (ed M G Ridpath & L K Corbett). Proceedings of the Ecological Society of Australia. Darwin Institute of Technology, Casuarina, NT, 13:203-214.

Heintzenberg J & E K Bigg 1990 Tropospheric transport of trace substances in the southern hemisphere, Tellus, 42B:355-363.

Herman B M, Box M A, Reagan J A & Evans C M 1981 Alternate approach to the analysis of solar photometer data. Applied Optics 20: 2925-2928.

Kondratyev K 1972 Radiation Processes in the Atmosphere. World Meteorological Organization, Report No.309, 214 pp.

McTainsh G H, Burgess R C & Pitblado J R 1989 Aridity, drought and dust storms in Australia (1960-1984). Journal of Arid Environments 16:11-22.

Middleton N J 1984 Dust storms in Australia: Frequency, distribution and seasonality. Search 15: 46-47.

Scientific Event Alert Network 1981 Bulletin of the Smithsonian Institution, Washington DC, Vol 6.

Scientific Event Alert Network 1982 Bulletin of the Smithsonian Institution, Washington DC, Vol 7.

Spinhirne J D 1984 El Chichon eruption cloud: latitudinal variation of the spectral optical thickness for October 1982. Geophysical Research Letters 9:881-884.

Voltz F E 1959 Photometer mit Selenphotoelement zur Bestimmung der Wellenlangenabhangigkeit der Dunsthaltung. Archiv Fuer Meteorologie, Geophysik und BioKlimatologie. B10:100-131.

Young A T 1981 On the Rayleigh-scattering optical depth of the atmosphere. Journal of Applied Meteorology 20:328-330.